ANTIMICROBIAL AGENTS AND CHEMOTHERAPY, Sept. 2009, p. 3860–3870 Vol. 53, No. 9
0066-4804/09/$08.00+0 doi:10.1128/AAC.00503-09

Target Analysis of the Experimental Measles Therapeutic AS-136A▽

Jeong-Joong Yoon,[1]† Stefanie A. Krumm,[1]† J. Maina Ndungu,[2] Vanessa Hoffman,[1] Bettina Bankamp,[3] Paul A. Rota,[3] Aiming Sun,[3] James P. Snyder,[3] and Richard K. Plemper[1,4]*

Department of Pediatrics, Emory University School of Medicine and Children's Healthcare of Atlanta, Atlanta, Georgia 30322[1]; Department of Chemistry, Emory University, Atlanta, Georgia 30322[2]; Division of Viral Diseases, Centers for Disease Control and Prevention, Atlanta, Georgia 30333[3]; and Department of Microbiology and Immunology, Emory University School of Medicine, Atlanta, Georgia 30322[4]

Received 16 April 2009/Returned for modification 19 May 2009/Accepted 8 June 2009

No effective therapeutic is currently in place for improved case management of severe measles or the rapid control of outbreaks. Through high-throughput screening, we recently identified a novel small-molecule class that potently blocks activity of the measles virus (MeV) RNA-dependent RNA polymerase (RdRp) complex in transient replicon assays. However, the nature of the block in RdRp activity and the physical target of the compound remained elusive. Through real-time reverse transcription-PCR analysis, we demonstrate that the lead compound AS-136A blocks viral RNA synthesis in the context of an infection. Adaptation of different MeV strains to growth in the presence of the compound identified three candidate hot spots for resistance that are located in conserved domains of the viral polymerase (L protein) subunit of the RdRp complex. Rebuilding of individual mutations in RdRp-driven reporter assays and recombinant MeV traced the molecular basis for resistance to specific mutations in L. Mutations responsible for resistance cluster in the immediate vicinity of the proposed catalytic center for phosphodiester bond formation and neighboring conserved domains of L, providing support for effective inhibition of a paramyxovirus RdRp complex through interaction of a nonnucleoside small-molecule inhibitor with the L protein. Resistance mutations are located in regions of L that are fully conserved among viral isolates, and recombinant MeV harboring individual resistance mutations show some delay in the onset of viral growth in vitro. Taken together, these data support the hypothesis that acquiring mutations in these L domains may reduce virus fitness.

In 2008, the highest measles case numbers in over a decade were observed in the United States and several European countries (6, 51, 52). For the United States, where the disease was declared eliminated in 2000 (37), this has been the result of greater viral transmission after importation of the virus (6). The United Kingdom, which is considered to have one of the worst measles rates in Europe, reported 1,217 cases from January to November 2008 alone (56). In June 2008, the virus was again declared endemic in the United Kingdom (18, 56), 14 years after it had been eliminated. Very high vaccination coverage rates (≥95%) are needed to interrupt transmission, due to the extremely infectious nature of measles virus (MeV) (38). The recent increase in measles cases in industrialized countries is considered to have arisen mostly as a consequence of elected exemption from vaccination because of philosophical or religious beliefs (6, 26). Complications of severe disease include encephalitis and pneumonia. Bacterial superinfections are frequently observed as a result of a prolonged immunosuppression of several months induced by the virus (22). Worldwide, there are approximately 200,000 measles deaths annually, rendering the virus a major cause for human morbidity and mortality from an infectious agent (7).

Despite the threat to human health, no licensed therapeutic is currently available for the treatment of measles. Conceivable areas of immediate use for effective anti-MeV agents include improved case management of acute disease and long-term neurologic complications, such as subacute sclerosing panencephalitis (20), resulting in reduced morbidity and mortality, rapid control of local outbreaks before vaccines and trained personnel are available or when vaccination is declined, and protection of the immunocompromised and infants prior to vaccination. In light of ongoing efforts toward global MeV control (32), safe, efficacious, and cost-effective antivirals would be a useful—and possibly essential—addition to our available arsenal against MeV. If global eradication of the virus will be attempted, antivirals embedded in a combined prophylactic (vaccination) and therapeutic (inhibitors) antimeasles platform could ensure that local outbreaks of the virus during a prolonged endgame of elimination, as experienced with poliovirus (25), will not result in expansive transmission.

MeV belongs to the myxovirus group, for which membrane-enveloped particles and negative-sense RNA genomes are characteristic (27, 39). Since host cells lack RNA-dependent polymerase activity, orthomyxoviruses, such as influenza virus, and paramyxoviruses, such as MeV, must encode their own RNA-dependent RNA polymerases (RdRp). These appear to be promising targets for antiviral therapies (13, 21, 35), since RdRp complexes assume a distinct structural configuration, their activity is essential for the virus life cycle, and a homologous cellular counterpart catalyzing the same activity does not exist. The last point opens the prospect of potent inhibition

* Corresponding author. Mailing address: Division of Infectious Diseases, Department of Pediatrics, 520 Children's Center, 2015 Uppergate Drive, Emory University School of Medicine, Atlanta, GA 30322. Phone: (404) 727-1605. Fax: (404) 727-9223. E-mail: rplempe@emory.edu.

† These authors contributed equally to the study.

▽ Published ahead of print on 15 June 2009.

without the penalty of inherent cytotoxic side effects of the drug. Despite these advantages, the development of nonnucleoside myxovirus RdRp inhibitors has been rather slow, and none of the currently licensed drugs belong to this class (13, 21). In contrast to antiretrovirals targeting reverse transcriptase, furthermore, little is known about paramyxovirus responses to RdRp inhibitors and the timeline for resistance to emerge.

Previously, we developed and implemented an automated drug screen for the identification of novel MeV inhibitors. Assessment of an ~34,000-entry small-molecule diversity set has yielded a novel compound class with target-specific nanomolar antiviral activity (57). Hit-to-lead chemistry has further advanced this compound class (53, 54), rendering it one of the most promising experimental MeV drugs identified. Initial mechanistic characterization has suggested inhibition of viral RdRp complex activity as causal for the antiviral effect (57). However, the molecular mechanism of antiviral activity and the physical target of the compound (i.e., viral nucleic acid, viral protein component, host cell factor, or a combination of factors) have not been defined.

As for other members of the paramyxovirus family, the MeV RdRp complex consists of three viral proteins, the nucleoprotein (N), the phosphoprotein (P), and the large protein (L), in addition to the RNA template. All enzymatic activity is considered to be located in the L subunit (27). The RdRp complex functions as the transcriptase and replicase for positive-sense-antigenome and negative-sense-genome synthesis (20, 27). Binding of L to the N-RNA nucleocapsid template occurs via L-P and P-N-RNA interactions, attributing a bridging function to the P protein (3, 12, 24, 48). In addition to viral components, cellular factors promote viral RNA synthesis (2, 33, 34).

Upon successful infection, incoming genomes serve as templates for RdRp-mediated synthesis of viral mRNAs. In addition to the ribonucleoprotein genome, infectious particles must thus harbor P and L proteins to initiate a replication cycle. *cis*-acting promoter and encapsidation signals required for transcription and replication are located in the noncoding termini of the viral genome (49). A subsequent switch in RdRp activity from transcription to RNA replication results in synthesis of full-length antigenomes, which then template the generation of progeny, negative-sense genomes (27).

In this study, we have explored whether the current lead entry of this experimental MeV drug class, AS-136A (53, 54), specifically blocks viral RNA synthesis in the context of an infection. Through virus adaptation, we have examined whether specific resistance clusters that highlight the physical target of the inhibitor and may, in a broader context, elucidate paramyxovirus response pathways to RdRp inhibitors can be identified. Having rebuilt candidate mutations individually in the context of genetically defined recombinant viral variants, we have furthermore explored whether resistance coincides with an altered growth profile compared to that of the drug-sensitive parental strain.

MATERIALS AND METHODS

Cell culture, compound synthesis, transfection, MeV strains, and production of MeV stocks. All cell lines were maintained at 37°C and 5% CO_2 in Dulbecco's modified Eagle's medium supplemented with 10% fetal bovine serum. Vero (African green monkey kidney epithelial) cells (ATCC CCL-81) stably expressing human signaling lymphocytic activation molecule (CD150w/SLAM), called in this study Vero-SLAM cells (36); baby hamster kidney (BHK-21) cells stably expressing T7 polymerase (BSR-T7/5 [BHK-T] cells) (4); and 293-3-46 cells stably expressing T7 polymerase and MeV N and P proteins (45) were incubated at every third passage in the presence of G-418 (Geneticin) at a concentration of 100 μg/ml. Chemical synthesis of compounds 16677 and AS-136A was achieved as previously described (53, 57). To prepare inhibitor stocks, compounds were dissolved at 150 mM in dimethyl sulfoxide (DMSO). Lipofectamine 2000 (Invitrogen) was used for cell transfections. MeV strains used in the study were recombinant MeV strain Edmonston, genotype A (recMeV-Edm) (45), and MeV isolates (MVi) MVi/Alaska.USA/16.00, genotype H2 (MVi-Alaska); MVi-Amsterdam.NET/49.97, genotype G2 (MVi-Ams); and MVi/Ibadan.NIE/97/1, genotype B3-2 (MVi-Ibd). All isolates were obtained from the WHO Strain Bank at the Centers for Disease Control and Prevention (47, 58). To prepare MeV stocks, Vero-SLAM cells were infected at a multiplicity of infection (MOI) of 0.001 PFU/cell and incubated at 37°C. Cells were scraped in Optimem (Invitrogen), virus was released by two freeze-thaw cycles, and titers were determined by 50% tissue culture infective dose ($TCID_{50}$) titration according to the Spearman-Karber method (50), as described previously (43).

Real-time RT-PCR. For quantitative reverse transcription-PCR (RT-PCR), Vero cells were infected with recMeV-Edm (45) in a six-well-plate format (MOI of 1.0). Thirty minutes postinfection, the virus inoculum was removed and AS-136A added at 5 μM or 25 μM. Controls received fusion inhibitory peptide (FIP) (Bachem) at 200 μM to prevent breakdown of the monolayer due to extensive cell-to-cell fusion prior to RNA extraction. Forty hours postinfection, plates were microphotographed and total RNA was extracted using an RNeasy mini kit (Qiagen). Cells in equally infected and treated parallel plates were subjected to immunodetection of F (see below). For RNA quantification, extracts were subjected to RT using Superscript II reverse transcriptase and antigenome-specific primer 5-GGCTCCCTCTGGTTGT (annealing to antigenome nucleotides 4962 to 4977 in reverse orientation), an oligo(dT) primer for mRNA quantification, or a random hexamer primer for cellular GAPDH (glyceraldehyde-3-phosphate dehydrogenase) or β-actin quantification. Real-time reactions were carried out using an Applied Biosystems 7500 Fast real-time PCR system and iQ SYBR Green supermix (Bio-Rad). The probe for antigenomic RNA was a 181-nucleotide amplicon at the N/P junction (primers 5-AACCAGGTCCACACAG and 5-GTTGTCTGATATTTCTGAC), the probe for F-encoding mRNA was a 209-nucleotide fragment (primers 5-GTCCACCATGGGTCTCAAGGTGAACG TCTC and 5-CAGTTATTGAGGAGAGTT), and the probe for GAPDH was a 160-nucleotide fragment (primers 5-CATGTTCGTCATGGGTGTGAACCA and 5-AGTGATGGCATGGACTGTGGTCAT). Melting curves were generated at the end of each reaction to verify amplification of a single product. To calculate $\Delta\Delta C_T$ values, threshold cycle (C_T) values obtained for each sample were normalized for GAPDH as a reference and then ΔC_T values of AS-136A-treated samples were normalized for the FIP-treated controls. Final quantification was based on three independent experiments in which each treatment condition and RT primer setting were assessed in triplicate. For visualization of RT-PCR products, larger fragments were amplified from the same cDNA templates by use of specific primers 5-TTCATGGTCGCTCTAATC and 5-GTTGT CTGATATTTCTGAC (1,131-bp N/P antigenome fragment), 5-CTACAAAGT TATGACTCG and 5-CGATAAACCAGATCTTTTCATACTCCTCAATATC TGGTCCG (1,353-bp F mRNA fragment), and 5-ATCTGGCACCACACCTT CTACAATGAGCTGCG and 5-CGTCATACTCCTGCTTGCTGATCCACAT CTGC (837-bp cellular β-actin fragment).

Immunodetection. For immunodetection of the viral F protein, infected cells were lysed with 10 mM HEPES, pH 7.4, 50 mM sodium pyrophosphate, 50 mM sodium fluoride, 50 mM sodium chloride, 5 mM EDTA, 5 mM EGTA, 1% Triton X-100, 1 mM phenylmethylsulfonyl fluoride, and protease inhibitors. Equal-size aliquots of cleared lysates (8,000 × *g*; 10 min; 4°C) were mixed with 2× urea buffer (200 mM Tris, pH 6.8, 8 M urea, 5% sodium dodecyl sulfate [SDS], 0.1 mM EDTA, 0.03% bromphenol blue, 1.5% dithiothreitol) and denatured for 25 min at 50°C. Samples were then fractionated on 10% SDS-polyacrylamide gels, blotted to polyvinylidene difluoride membranes (Millipore), and subjected to enhanced chemiluminescence detection (Pierce) using a polyclonal antiserum directed against the F cytosolic tail, as previously described (28).

Virus adaptation. For the generation of resistant strains, Vero-SLAM cells were infected with MeV-Edm, MVi-Alaska, MVi-Ams, or MVi-Ibd at an MOI of 0.1 PFU/ml and incubated in the presence of increasing 16677 (57) or AS-136A concentrations starting at 0.5 μM. When extensive cell-to-cell fusion was detected, cell-associated viral particles were released by two freeze-thaw cycles, diluted 10-fold, and used for infection of fresh cell monolayers in the presence of compound at increasing concentrations. Virus was subjected to two consecutive rounds of plaque purification when virus-induced cytopathicity was readily de-

tectable in the presence of 30 μM compound. Purified clones were reassessed for resistance, evidenced by cytopathic-effect (CPE) formation in the presence of ≥30 μM compound.

cDNA sequence analysis of adapted and recombinant viral variants. cDNA fragments were generated from Vero-SLAM cells infected with confirmed adapted clones or rebuilt, recombinant MeV variants by use of random hexamer primers as described above. For sequencing of the N-, P-, and L-encoding open reading frames, the noncoding intergenic domains between N and P, P and M, and H and L and the noncoding leader and trailer sequences of genome cDNA fragments were further amplified using *Pfu*-Ultra polymerase (Stratagene). The first 20 nucleotides of the 3′ genomic terminus and the last 21 nucleotides of the 5′ terminus were not examined. A fragment containing the leader-N-P region and two overlapping fragments containing the L-trailer region were amplified using primers based on the sequence of EdmBil (GenBank accession number Z66517). Reverse transcriptase reactions were performed using Superscript II reverse transcriptase (Invitrogen). PCR was performed with Elongase enzyme mix (Invitrogen) according to the manufacturer's recommendations for long PCR. Fragments were sequenced with a Big Dye Terminator v1.1 cycle sequencing kit (Applied Biosystems), using primers based on the EdmBil sequence. Primer sequences are available upon request. All sequence data were analyzed with the Sequencher program (Gene Codes Corporation).

Plasmid generation and mutagenesis. For directed mutagenesis of components of the MeV-Edm RdRp complex, plasmids harboring the L, N, or P open reading frame under the control of the T7 promoter (49) were used as starting material. Individual primer sequences are available upon request. A firefly luciferase MeV replicon reporter construct was generated by double-recombination PCR using plasmids luciferase T7 control DNA (Promega) containing the luciferase gene and MeV chloramphenicol (CAT) minigenome reporter (49) as templates. Primers were 5-**CTTTATGTTTTTGGCGTCTTCCAT**CTCGGATAT CCCTATATCC and 5-**GGCGGAAAGTCCAAATTGTAA**TTGGTTGAACTCC GGAACC (luciferase gene-specific sequences are highlighted in bold) for recombination and appropriate flanking primers (sequences available upon request). Following both recombination steps, the amplicon was subcloned into the pCR 2.1-TOPO vector (Invitrogen), and an AgeI/AvrII fragment containing the luciferase gene was transferred into the equally digested CAT MeV replicon plasmid, thus replacing the CAT gene while leaving sequences flanking the open reading frame unchanged.

RdRp reporter assays. BHK-T cells (2.5×10^5 per well in a 12-well-plate format) were transfected with plasmid DNAs encoding the MeV-L (0.24 μg), MeV-N (0.94 μg), or MeV-P (0.29 μg) variant and 2 μg of the MeV CAT or luciferase replicon reporter plasmid. Control wells included identical amounts of reporter and helper plasmids but lacked the plasmids harboring the respective L gene. Two hours posttransfection, compound AS-136A was added, while controls received solvent (DMSO) only for comparison. Thirty-eight hours posttransfection, cells were lysed and CAT concentrations or luciferase activities in the lysates were determined using a CAT enzyme-linked immunosorbent assay system (Roche) or Bright-Glo luciferase substrate (Promega) and an Envision multilabel microplate reader (Perkin Elmer), respectively. The statistical significance of results was determined using Student's *t* test.

Recovery of recombinant viruses. Recombinant MeV were generated essentially as described previously (45). Briefly, the helper cell line 293-3-46 was transfected with a cDNA copy of the relevant MeV genome and MeV polymerase L by calcium phosphate precipitation using a ProFection kit (Promega). Helper cells were overlaid on Vero-SLAM cells 76 h posttransfection and emerging infectious particles transferred to fresh Vero-SLAM cells. The integrity of recombinant MeV particles was confirmed by RT-PCR and DNA sequencing of the modified area.

Viral CPE reduction assay. To test the sensitivity of virus variants to compound-mediated inhibition, Vero-SLAM cells were infected in four replicates per compound concentration in a 96-well-plate format at an MOI of 0.4 PFU/cell in the presence of AS-136A ranging from 37.5 μM to 9.375 μM in twofold dilutions. At 96 h postinfection, cell monolayers were subjected to crystal violet staining (0.1% crystal violet in 20% ethanol) and dried plates photodocumented. For quantitative analysis, absorbance of dried plates at 560 nm was determined and virus-induced cytopathicity calculated according to the following formula: percent relative CPE = 100 − (unknown sample − minimum)/(maximum − minimum) × 100, with minimum referring to infected, vehicle-treated wells and maximum to mock-infected wells.

Viral growth profiles. For multistep growth curves, cells were infected in a six-well-plate format with MeV-Edm variants at an MOI of 0.01 PFU/cell. To ensure equal MOIs for all variants analyzed, all input stocks were prediluted to approximately 10^4 $TCID_{50}$/ml in Optimem (Invitrogen) prior to infection, and titers were reconfirmed by $TCID_{50}$ titration. Sixty minutes postinfection, inocula were replaced with fresh growth medium. Cell-associated viral particles were harvested every 12 h as described above and subjected to $TCID_{50}$ titration.

Virus yield reduction assay. To assess viral resistance to inhibition based on reduction of titers of infectious particles, 2×10^5 cells per well were infected in a 12-well-plate format with MeV variants at an MOI of 0.1 PFU/cell in the presence of a range of compound concentrations (50 μM, highest) or equivalent volumes of solvent (DMSO) only and incubated in the presence of compound at 37°C. Thirty-six hours postinfection, cell-associated viral particles were harvested and titers were determined as described above. Plotting virus titers as a function of compound concentration allowed a quantitative assessment of resistance. Where applicable, 50% inhibitory concentrations were calculated using the BioDataFit 1.02 (Chang Bioscience) or Microsoft Excel software package.

RESULTS

Since we have identified in previous work a novel class of experimental nonnucleoside MeV drugs that specifically interfere with activity of the viral RdRp complex in transient minireplicon-based reporter assays (57), it was the overall goal of this study to further assess the mechanism of antiviral activity and determine the target molecule of this inhibitor class.

AS-136A specifically blocks synthesis of viral RNA in infected cells. To examine whether the novel inhibitor class specifically blocks viral RNA synthesis in the context of an infection, we measured MeV mRNA and antigenome (positive-sense-RNA) levels in recMeV-Edm-infected, inhibitor-treated Vero cells by real-time RT-PCR. For all experiments, the class-defining lead analog compound AS-136A (53) (structure depicted in Fig. 1A) was used. Since the compound effectively suppresses the generation of progeny virus, cells were infected with an MOI of 1.0 to ensure a high primary-infection rate. Vehicle controls received FIP, a synthetic tripeptide blocking MeV glycoprotein-mediated membrane fusion (19), to prevent breakdown of the monolayer prior to RNA extraction due to extensive cell-to-cell fusion (Fig. 1B), the hallmark CPE associated with MeV infection in cell culture (20).

The majority of paramyxovirus mRNAs are monocistronic, since readthrough transcription that ignores intergenic polyadenylation/termination signals is generally infrequent (27). To fully exclude contamination of the full-length RNA signal with incoming (negative-sense) genomic RNA or bicistronic mRNAs, an antigenome-specific primer was used to initiate cDNA synthesis, and a probe fragment that is located three intergenic junctions upstream of the primer binding site was amplified. Although a higher readthrough frequency is detected at the MeV M-F junction (5), this primer setup mandates a triple readthrough (N-P-M-F) polycistronic messenger to yield an mRNA-based signal. To quantify viral mRNA levels, a fragment of the F gene was amplified, following cDNA priming with poly(dT) oligonucleotides.

Relative quantitations through calculation of $\Delta\Delta C_T$ values demonstrated dose-dependent, potent (100-fold to 1,000-fold, depending on the compound concentration examined) reductions of both viral mRNA and antigenomic RNA levels by AS-136A (Fig. 1C). Immunoblotting of the viral F protein (Fig. 1D) and assessment of viral CPE prior to RNA extraction (Fig. 1B) confirmed that this ~100-fold reduction in RNA signal achieved by 5 μM compound was sufficient to render F protein undetectable biochemically and completely block cell-to-cell fusion.

These findings demonstrate the effective suppression of RNA synthesis by AS-136A also in the context of virus infec-

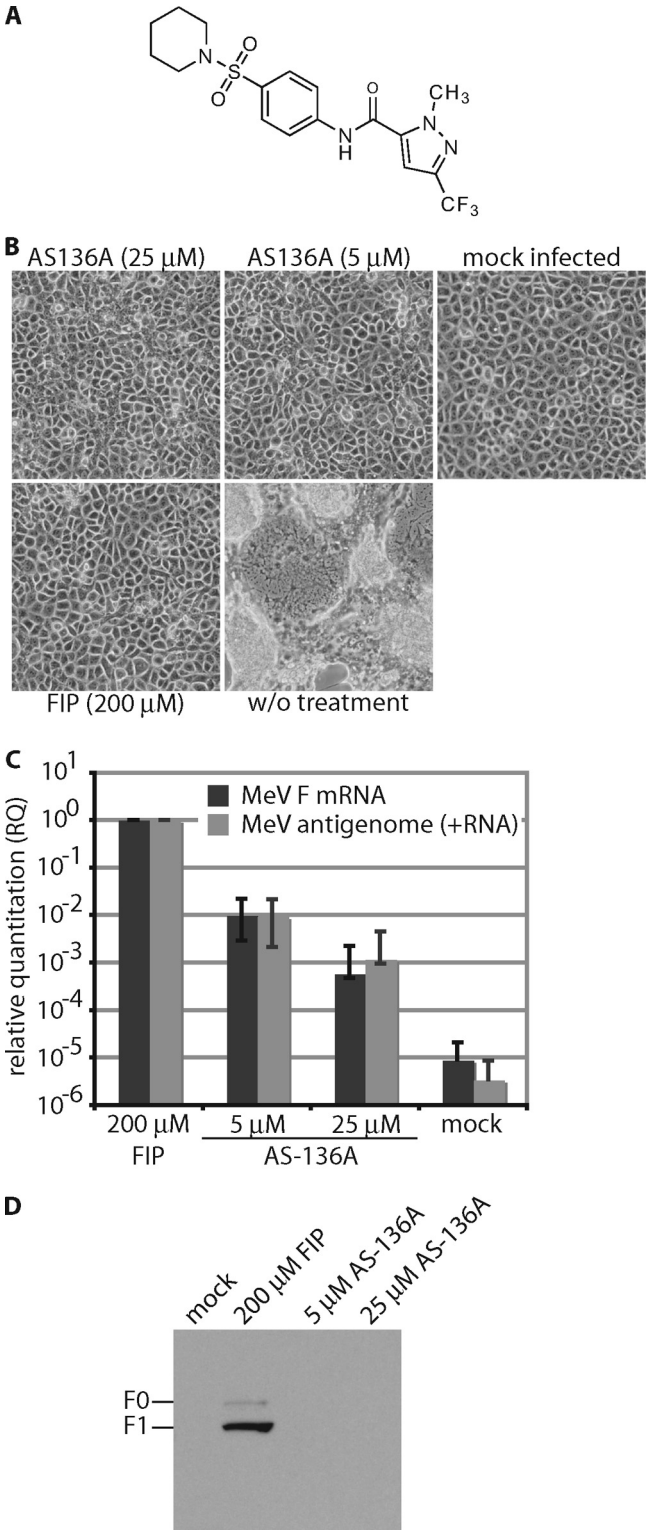

FIG. 1. Lead compound AS-136A inhibits MeV RNA synthesis in the context of virus infection. (A) Structure of AS-136A, first described in reference 53. (B) Microphotographs of Vero-SLAM cells infected with MVi-Alaska at an MOI of 1.0 and treated with different concentrations of AS-136A or FIP as indicated. The compound efficiently blocks virus-induced cytopathicity (cell-to-cell fusion). Mock-infected cells received infection media without virus; aliquots of both mock-infected cells and untreated cells ("w/o treatment") were exposed to equivalent maximum concentrations (0.02%) of vehicle (DMSO) only. Images were taken 24 h postinfection at a magnification of ×100. (C) Relative quantitations of F mRNA and positive-sense-antigenome (+RNA) levels in cells shown in panel B, determined using real-time RT-PCR. AS-136A-exposed samples were normalized to levels for FIP-treated cells, and $\Delta\Delta C_T$ values were calculated using cellular GAPDH as the reference. Averages from three independent experiments, each assessed in triplicate, are shown. Error bars represent standard deviations. (D) Western analysis of the F-protein contents of cells shown in panel B. Cleared lysates of cells were fractionated by SDS-polyacrylamide gel electrophoresis, and F antigenic material was detected by immunoblotting using a specific antiserum directed against the cytosolic F tail. Immature F_0 and proteolytically matured F_1 fractions are highlighted.

TABLE 1. Active concentrations of class-identifying compound 16677 and current lead analog AS-136A against wild-type and attenuated MeV strains of different genotypes used in this study

MeV strain (reference)	Genotype	50% inhibitory concn (μM)[a]	
		Compound 16677[b]	Analog AS-136A
MVi-Alaska (41)	H2	0.035 ± 0.003	0.027 ± 0.024
MVi-Ams (41)	G2	0.05 ± 0.03	0.01 ± 0.001
MVi-Ibd (41)	B3-2	0.14 ± 0.03	0.04 ± 0.015
recMeV-Edm (45)	A	0.024 ± 0.01	0.37 ± 0.2

[a] Values represent means derived from at least three independent concentrations ± standard deviations.
[b] See reference 57.

tion, confirming inhibition of RdRp complex activity as the basis for antiviral activity.

Target identification through induction of viral resistance. To determine the target of the compound, i.e., viral protein or nucleic acid or cellular cofactors required for RdRp activity, we generated resistant viral variants through stepwise adaptation to growth in the presence of compound. Attenuated and wild-type MeV strains representing four different genotypes (A, H2, G2, and B3) (47) served as input strains, and the class-identifying compound 16677 or the current lead AS-136A was used. Efficient inhibition of MeV strains of all four genotypes, previously observed for compound 16677 (57), was first confirmed for analog AS-136A through generation of virus yield-based dose-response curves and calculation of 50% inhibitory concentrations (Table 1). Figure 2A shows the profiles for 13 independent adaptations. We considered viral variants adapted when they tolerated an inhibitor concentration of 30 μM, evidenced by the readily apparent viral CPE in infected cells.

Following plaque purification, resistance was reconfirmed in comparison with that for the different input strains through assessment of CPE suppression by AS-136A (Fig. 2B). Twelve of the 13 variants revealed robust resistance in this assay, while variant Edm-1* (the asterisk indicates that the virus was exposed to 16677) showed an intermediate phenotype. However, the other three variants exposed to 16677 for adaptation (Alaska-1*, Alaska-2*, and Edm-2*) returned robust resistance against AS-136A in this assay, supporting a common mechanism of activity of the class-identifying compound and the current lead analog. As we have reported earlier, MVi-Ibd is naturally re-

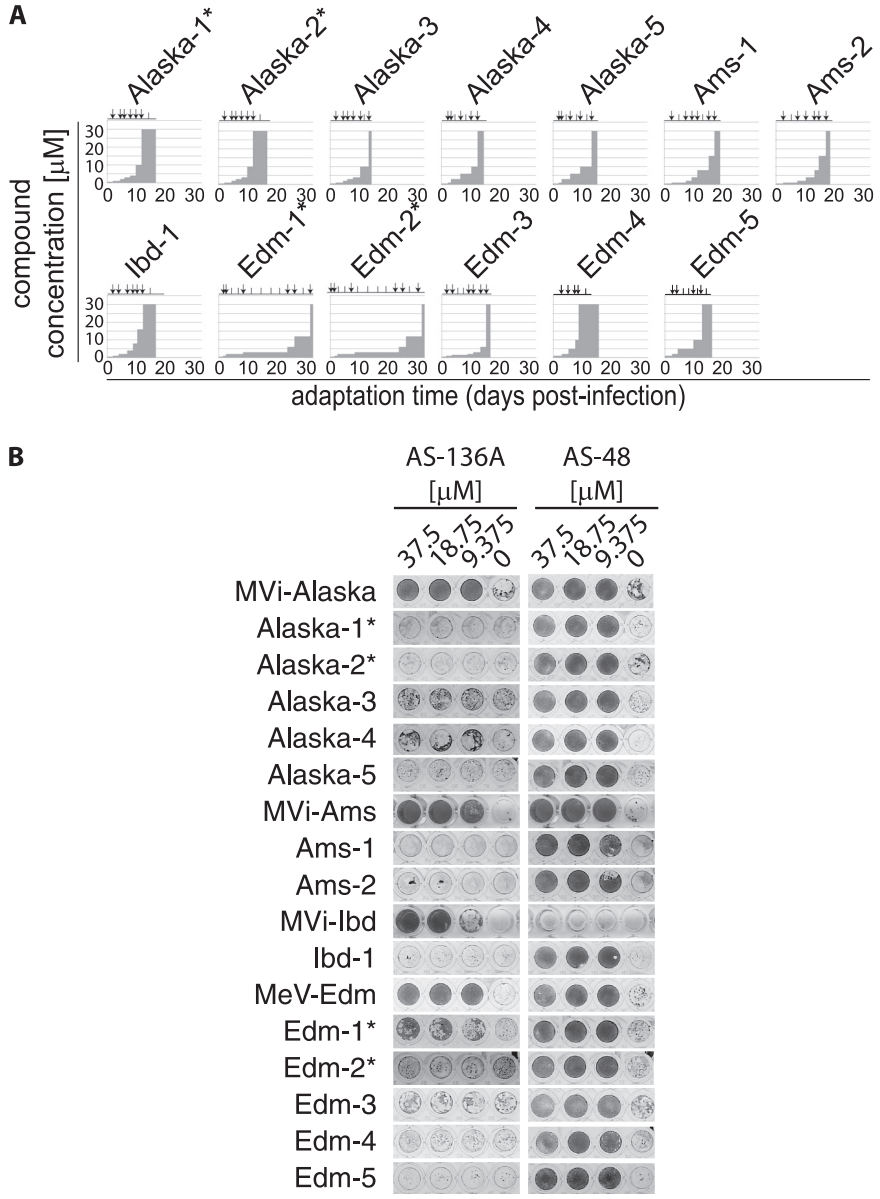

FIG. 2. Specific resistance to the AS-136A class emerges in stepwise adaptations after 13 to 31 days. (A) Profiles of 13 adaptations, covering four different strains. Viruses marked with an asterisk were exposed to the class-identifying hit compound 16677, and all others were exposed to the lead analog AS-136A. Vertical arrows indicate harvest times of cell-associated viral particles, followed by infection of fresh target cells, and vertical lines mark passages of infected cells. (B) Twelve adapted clonal variants show high-level resistance to AS-136A in a viral CPE suppression assay, while MeV-Edm-1* displays intermediate resistance. None of the adapted variants is resistant to the MeV entry inhibitor AS-48 (41, 42). Cells were infected with clonal MeV variants (four replicates/variant) at an MOI of 0.4 in the presence of different AS-136A or AS-48 concentrations, followed by crystal violet staining and photodocumentation of cell monolayers 4 days postinfection. Representative dilution series are shown. Input strains used for adaptation were included for reference.

sistant to the entry inhibitor AS-48, a small-molecule compound specifically targeting the MeV fusion envelope protein that we have developed and characterized in previous studies (16, 44). We note, however, that adapted Ibd-1, which is resistant to AS-136A, was sensitive to AS-48 (Fig. 2B). The natural resistance of MVi-Ibd to AS-48 is due to an N462K point mutation in the F protein (16), which is present in a quasispecies in MVi-Ibd. Partial F sequence analysis confirmed that only the standard, AS-48-sensitive F protein 462N allele is present in the AS-136A-resistant Ibd-1 clone (data not shown).

Most variants achieved this status of resistance in less than 20 days. In two cases (MeV-Edm-1* and MeV-Edm-2*), generation of robust resistance required approximately 30 days. In both cases, the original hit 16677 was combined with attenuated MeV-Edm, which is the least sensitive to this compound class of all MeV strains tested (57). Longer adaptation times may thus reflect lower selective pressure in these settings than realized with the other combinations. Resistance was specific for the RdRp inhibitor compound class and did not extend to the small-molecule MeV fusion inhibitor AS-48 (Fig. 2B).

Taken together, the selective resistance profile and adaptation timeline support specific targeting of viral factors by the compound while arguing against interference with host factors required for RdRp activity.

Individual point mutations in the L protein mediate resistance in a replicon assay. All purified clones with confirmed resistance were subjected to RT-PCR and DNA sequencing to identify candidate mutations that may mediate the phenotype. For all eight MVi-Alaska, -Ams, and -Ibd-based variants and one MeV-Edm strain, the sequences of the N-, P-, and L-encoding open reading frames; the N-P, P-M, and H-L intergenic junctions; and the 5′and 3′ untranslated leader and trailer sequences of the viral genomes were compared with the sequences of the corresponding input viruses. The first 20 nucleotides of the 3′ genomic terminus and the last 21 nucleotides of the 5′ terminus, which were previously found to be fully conserved (29), were not examined.

None of the resistant variants showed changes in the leader or trailer domain, and only a small number of scattered mutations was observed in the N, P, C, or V reading frame of some variants (Fig. 3A). In contrast, three distinct mutation clusters became readily apparent when the L open reading frame was examined. Each was defined by coding changes less than 10 amino acids apart and present in at least two different genotypes (Fig. 3A, positions 589, 768/776, and 1233/1239). With the exception of MVi-Alaska-4, which showed no overlap with any of the other clones examined, each of the adapted variants harbored a mutation in one of these clusters.

Clustering suggested a direct involvement of residues located in these areas in the development of resistance. We hence limited sequence analysis of the remaining four MeV-Edm-based clones (MeV-Edm-2* to MeV-Edm-5) to an area in the L open reading frame approximately corresponding to residues 270 to 1300. In each of these MeV-Edm variants, a mutation that was clearly attributable to one of the clusters was found (Fig. 3A).

Starting with the residues located in these areas, we rebuilt a subset of L mutations individually in an expression plasmid encoding MeV-Edm L. Analysis of bioactivity of the resulting constructs in an MeV minireplicon reporter assay in the presence of AS-136A confirmed that a single change in either of these clusters mediated full resistance (Fig. 3B). This was further accentuated by the observation that neither of the additional point mutations examined that was located outside of the cluster zones contributed to resistance. The only exceptions were the adapted strains Alaska-4 and Edm-1*. The former harbored no mutation in any cluster zone. Instead, we found the L1170F change in the L protein [designated L(L1170F)] of Alaska-4 fully responsible for resistance (Fig. 3B). For the latter, rebuilding of mutation R1233Q had no effect in the single-concentration (30 μM) replicon assay. However, the base RdRp activity level in the absence of compound was approximately 120% of that in the unmodified system when L(R1233Q) was present. Furthermore, MeV-Edm-1* harbors an M502V change in the P protein in addition to the L(R1233Q) mutation. To examine whether higher base activity and/or multiple mutations contribute to resistance of this variant, we also rebuilt the M502V mutation in the P expression plasmid and generated replicon-based dose-response curves for all combinations of mutant and unmodified L and P constructs (Fig. 3C). These revealed that starting from a higher activity base expands the compound concentration window in which RdRp activity is detectable, resulting in intermediate-level resistance. Sensitivities of mutant and parent RdRp complexes to AS-136A remained unchanged, however, as evidenced by equal slopes of the dose-response curves. The P(M502V) mutation alone or in combination with L(R1233Q) did not contribute to the resistance phenotype.

Taken together, the data from the replicon assay attributed resistance in all 13 cases to distinct point mutations in L. Although input strains represented different MeV genotypes, the resistance phenotype for all of these could be recapitulated in the MeV-Edm-based replicon system. This demonstrates that the effect of the individual mutations is independent of the genetic origin of L. The high degree of redundancy of confirmed mutations mediating escape from AS-136A among independently adapted clones supports the notion that major hot spots for resistance to the compound class have been identified.

Mechanisms of resistance. In contrast to L(R1233Q) in MeV-Edm-1*, all other confirmed mutations in cluster areas or at L position 1170 induced high-level resistance in the replicon assay, while baseline RdRp activities remained essentially unchanged, indicating reduced sensitivity to the compound. Rebuilding these mutations individually in the genetically controlled background of recombinant MeV-Edm further supported this notion. In contrast to the efficient inhibition of the genetic parent virus (recMeV-Edm), yields of each of the recombinants were unchanged even after growth in the presence of 50 μM AS-136A, which is the highest compound concentration that remains fully in solution in growth medium for the duration of the assay. This degree of resistance corresponds to a >135-fold reduction in sensitivity to the drug (Fig. 4).

Figure 4 furthermore confirms that the intermediate resistance observed for the Edm-1* L(R1233Q) variant in the replicon system extends to the context of virus infection. As with the transient replicon assay, clonal MeV-Edm-1* displayed an intermediate phenotype, characterized by an ~12-fold increase in 50% inhibitory concentration. Given that the Edm-1* variant was derived from adaptation of recMeV-Edm, achieved only intermediate resistance, and harbored solely the P(M502V) and L(R1233Q) mutations in its RdRp components, we did not generate a recMeV-Edm L(R1233Q) variant de novo. These data indicate that MeV escape from the AS-136A inhibitor class can be achieved through two distinct mechanisms. Increased RdRp base activity results in intermediate-level resistance, with ~12-fold-higher inhibitory concentrations. Unchanged RdRp activity levels but reduced sensitivity to the drug mediates high-level resistance.

Resistance mutations cluster in conserved domains of L. Through sequence comparisons, six distinct and highly conserved domains have previously been identified in the paramyxovirus L protein (27). Overlaying confirmed mutations mediating resistance to AS-136A onto the MeV L domain structure revealed that all of the changes localize in domain II, III, or IV (Fig. 5A). While no distinct function has been attributed to domain IV yet, domain II is postulated to have RNA-binding activity (27) and domain III is thought to harbor the site for polymerization. In fact, MeV L residues 768 and 776 closely frame a conserved GDNQ motif in domain III,

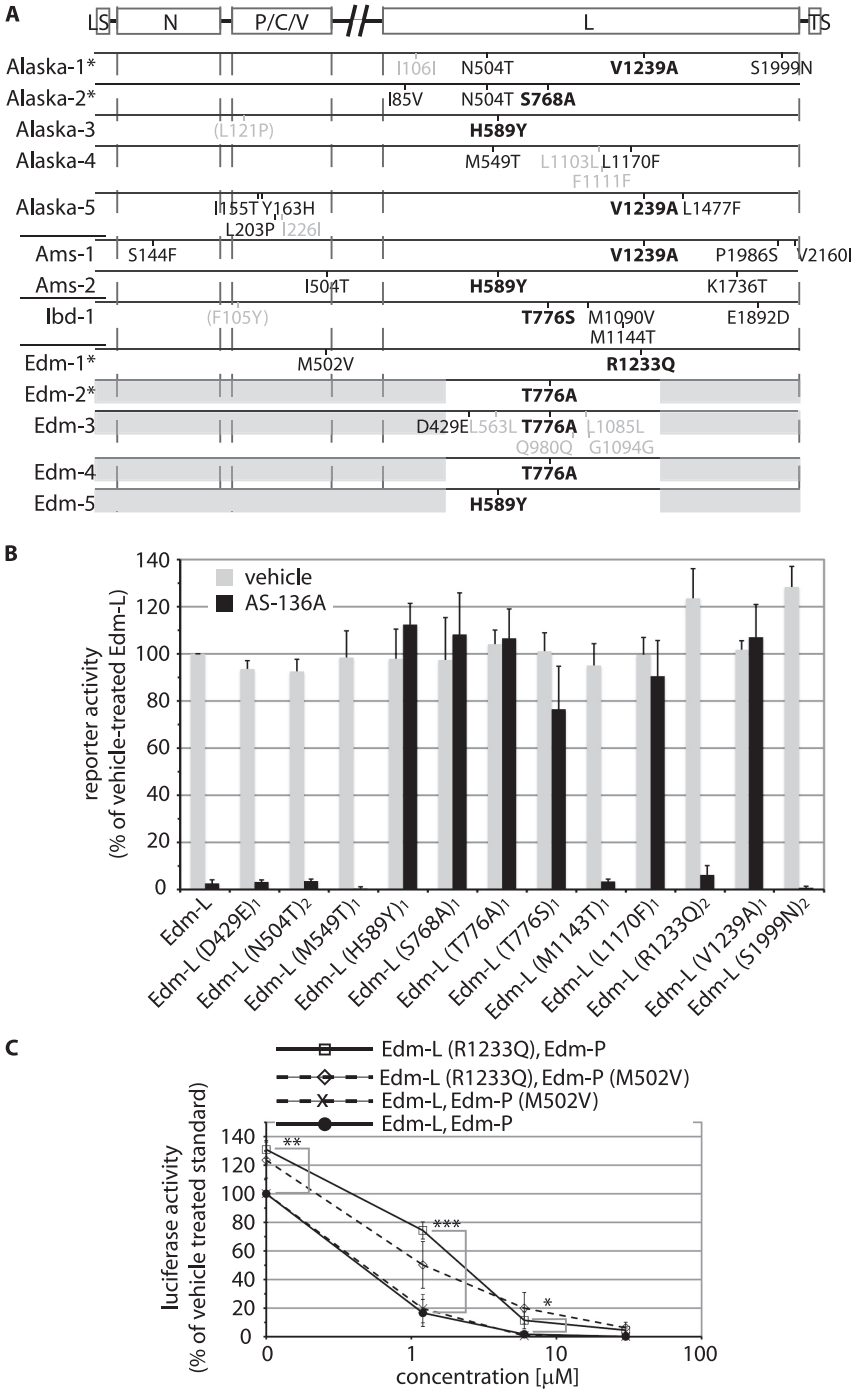

FIG. 3. Identification of mutations causal for resistance. (A) Sequence analysis of the noncoding genomic termini (LS and TS), intergenic regions, and viral N, P/C/V, and L proteins of the 13 resistant MeV clones in comparison with those of the respective sensitive input strains. Envelope components located between the P and L open reading frames were not examined. Coding changes in viral structural proteins are marked in black, silent mutations are shown in gray, and changes in the nonstructural C protein are displayed in parentheses. Three mutation cluster zones were identified (changes are shown in bold). Noncoding regions were unchanged in all cases. Shaded areas for MeV-Edm variants were not sequenced. (B) With the exception of Edm-1*, a transient MeV replicon reporter assay identified for each adapted clone a single mutation in L that reconstitutes complete resistance. Selected candidate mutations were rebuilt individually in an MeV-Edm L expression plasmid, and RdRp-driven reporter activity was assessed upon transfection of replicon-encoding plasmids into BHK-T cells and incubation in the absence or presence of 30 μM AS-136A. Values are normalized for those obtained with the unmodified replicon system in the absence of AS-136A and represent averages from at least three independent experiments ± standard errors. Results are based on a CAT (constructs marked "1") or an identical firefly luciferase (constructs marked "2") reporter. (C) Dose-response curves demonstrate higher base RdRp activity in the replicon assay when the L(R1233Q) mutation (found in Edm-1*) is present, resulting in intermediate-level resistance. The luciferase-based MeV reporter was used for all experiments; values were normalized as described for panel B and represent averages from seven independent experiments ± standard errors of the means. Asterisks represent P values derived from t test analysis (***, $P < 0.001$; **, $P < 0.01$; *, $P < 0.05$).

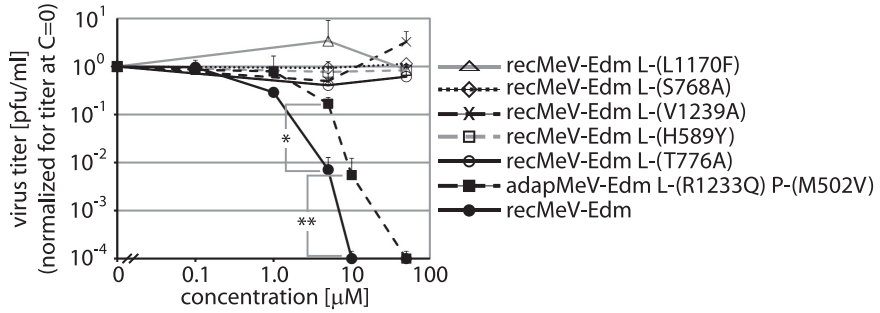

FIG. 4. Two distinct resistance profiles are found in the context of virus infection. Clonal, adapted MeV-Edm-1* (adapMeV) shows intermediate-level resistance, while all other replicon-confirmed L mutations mediate high-level (>135-fold) resistance. For the latter, individual L mutations were rebuilt in a cDNA copy of the MeV genome and recombinant MeV was recovered. Vero cells were then infected with these variants or unmodified recMeV-Edm for comparison in the presence of different AS-136A concentrations or vehicle control (concentration [C] = 0) at an MOI of 0.1. Cell-associated viral particles were harvested 30 h postinfection and subjected to $TCID_{50}$ titration. Averages from three independent experiments ± standard deviations are shown. Asterisks represent *P* values derived from *t* test analysis for adapMeV-Edm L(R1233Q) P(M502V) (**, $P < 0.01$; *, $P < 0.05$).

which is considered the catalytic center for phosphodiester bond formation (10, 11, 27).

Sequence comparison of the L proteins of representative wild-type MVi and the attenuated MeV-Edm strain revealed complete conservation of each of the six residues involved in resistance to AS-136A and the surrounding microdomains (Fig. 5B). Natural variations at these positions were detected when the comparison was expanded to other paramyxoviruses. However, the biochemical properties of the side chains of homologous residues were frequently conserved (Fig. 5B).

To examine whether the resistance mutations affect MeV growth in cell culture, we generated multistep growth curves for clonal Edm-1*, the panel of MeV recombinants harboring point mutations in L, and parental recMeV-Edm. All variants reached final virus titers equivalent to those for recMeV-Edm. However, different growth patterns were observed. The recMeV-Edm L(L1170F) variant and clonal Edm-1* returned a largely recMeV-Edm-like growth profile, revealing, if anything, a slight delay at the onset of growth (Fig. 5C, top). Thus, higher base RdRp levels in the transient replicon assay for L(R1233Q) (present in clonal Edm-1*) did not translate into accelerated viral growth in cell culture. For the recMeV-Edm L(S768A), L(T776A), and L(V1239A) variants, the onset of proliferation was delayed by approximately 12 h. Then, growth rates were similar to or even slightly higher than that for recMeV-Edm (Fig. 5C, middle). The recMeV-Edm L(H589Y) variant likewise showed a 12-h delay before progeny virus was detectable. However, this was combined with growth rates that were lower than that for the parent strain, resulting in an approximately 12- to 24-h delay until plateau titers were reached (Fig. 5C, bottom).

Thus, most mutations resulting in robust resistance were linked to an initial delay in viral growth in cell culture, albeit to various degrees. Complete conservation of specific residues involved in resistance and the surrounding microdomains in all genotypes examined furthermore indicates that natural selective pressure to maintain the molecular nature of these amino acids exists.

DISCUSSION

Nonnucleoside inhibitors of RNA virus RdRp complexes constitute attractive targets for antiviral therapy since they combine the potential for potent inhibition of virus replication with a low intrinsic propensity for side effects. Consistent with this general concept, the previously identified AS-136A class of small-molecule MeV inhibitors exudes low cytotoxicity but efficiently suppresses RdRp activity in transient replicon assays (53, 54, 57). To assess the full developmental potential of this compound class and, by extension, small-molecule drugs with an equivalent mechanistic profile directed against other paramyxovirus family members, the mechanism of inhibition in the context of viral infection, the target of the compound, and viral escape strategies must be determined.

Quantitative RT-PCR analysis of viral mRNA and antigenomic full-length RNA in this study clearly demonstrated a dose-dependent inhibition of MeV RdRp activity in the context of viral replication. Stepwise adaptation of four MeV strains representing different genotypes has demonstrated that under optimized conditions (compound dosed to impair but not fully suppress virus replication) robust resistance emerges after four to six virus passages and a cumulative incubation time of approximately 10 to 20 days. This rapid adaptation pattern is consistent with that observed for nonnucleoside reverse transcriptase inhibitors (NNRTI) used in antiretroviral therapy (17, 31, 46) and is characteristic of a pathogen-directed rather than a host factor-directed mechanism of antiviral activity. For the latter, longer adaptation times and less robust, if any, resistance are postulated, since mammalian cells do not mutate rapidly and viral mutations may not restore functionality of an inhibited host factor that is required for completion of the viral life cycle (55).

cDNA sequencing of the viral RdRp components and noncoding terminal regions of the genome highlighted three prominent mutation clusters in the L protein. In 12 of 13 adapted virions, changes in one of these cluster zones were found. This degree of redundancy suggests that major hot spots of resistance have been identified. Two lines of evidence create confidence that independently emerged viral variants were exam-

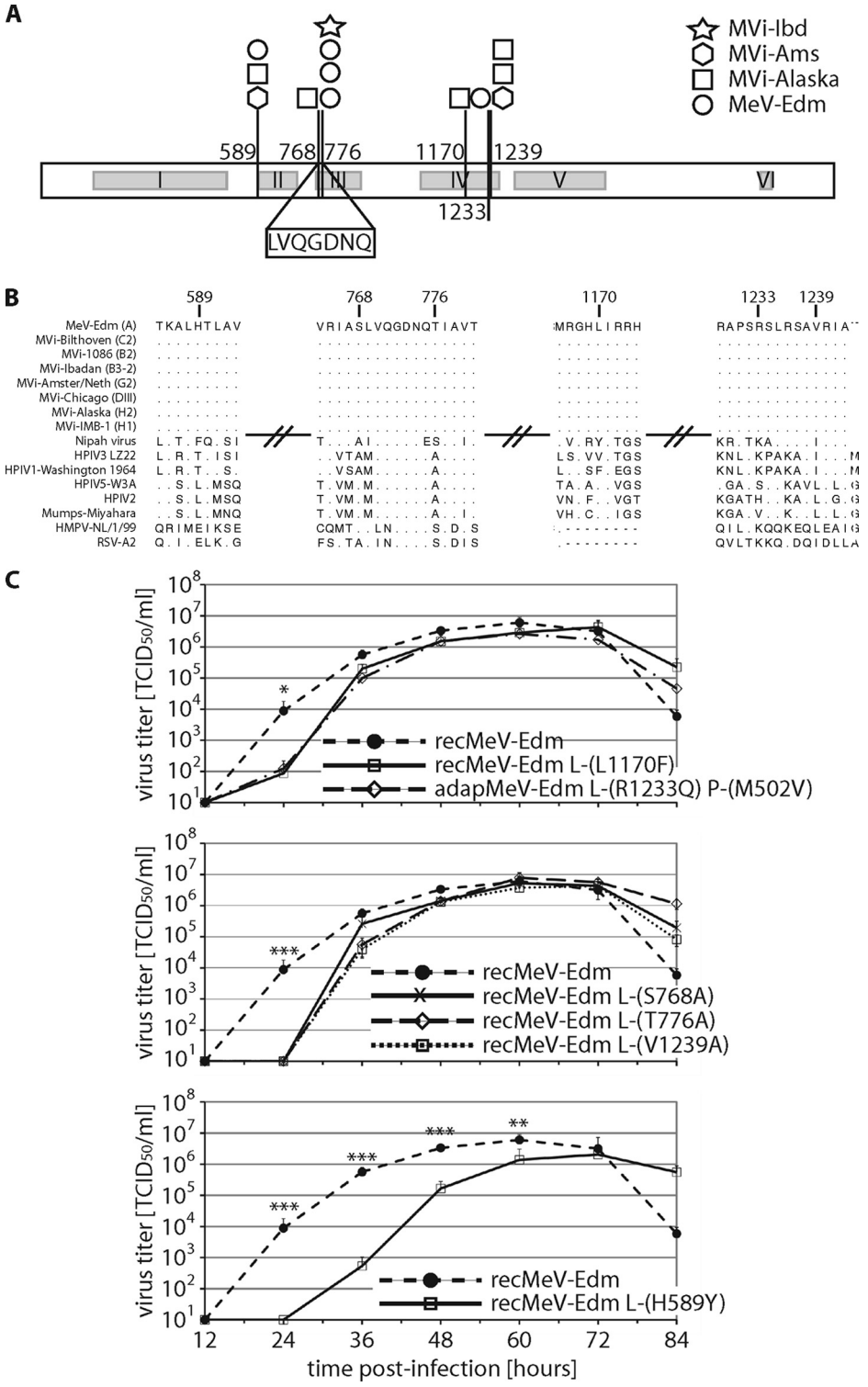

FIG. 5. Resistance mutations cluster in conserved domains of MeV L. (A) Schematic of MeV L, depicting the positions of confirmed mutations relative to six previously described conserved domains in L (domains I to VI, gray boxes). The position of the GDNQ motif, postulated as the active center for polymerization, is indicated. Each symbol represents an independently adapted clone. (B) L sequence alignment for selected MeV strains representing different genotypes and a set of additional paramyxovirus family members. Areas surrounding the six residues implemented in resistance (identified above the sequences) are shown. Strain names are provided when available, and viral genotypes are given in parentheses. HPIV, human parainfluenzavirus; HMPV, human metapneumovirus; RSV, respiratory syncytial virus. (C) Recombinant MeV with high-level resistance mutations show three distinct growth patterns. Vero cells were infected with recMeV-Edm, different recMeV-Edm variants, or clonal, adapted MeV-Edm-1* (adapMeV), and titers of cell-associated viral particles were determined at the indicated time points, as described in the legend for Fig. 4. Unmodified recMeV-Edm was included for comparison. Average values from at least six (recMeV-Edm and recMeV-Edm variants) or three (adapMeV) independent experiments ± standard errors of the means are shown. Asterisks represent P values for early time points of each growth curve, derived from t test analysis (***, $P < 0.001$; **, $P < 0.01$; *, $P < 0.05$); for graphs showing multiple mutant viral variants, P value symbols correspond to the variant for which the lowest statistical significance was calculated.

ined: equivalent changes were found in adapted variants of different MeV genotypes or, when viruses of the same genotype were compared, in variants with an otherwise unique background pattern of random mutations.

Rebuilding individual mutations in L expression plasmids confirmed a causal link to the resistance phenotype and highlighted two strategies of escape from inhibition. L(R1233Q) (variant Edm-1*) resulted in intermediate-level resistance in the replicon assay and in the context of virus infection. In the replicon assay, this mutation increased the base activity level of the RdRp complex, suggesting higher catalytic activity as a basis for expanded drug tolerance. L residue 1233 is located in conserved domain IV, for which no defined function has been proposed. Of all possibilities, this residue is not likely a candidate for altering RdRp complex stability through short-range interactions, since L-P binding domains (8, 23, 40) and L-L oligomerization domains (8, 9) have been mapped to N-terminal domains of L.

In contrast to Edm-1*, the majority of variants identified showed high-level resistance in the replicon assay and in the context of genetically controlled, recombinant MeV, while retaining largely unchanged RdRp activity levels. This pattern is characteristic of a reduced affinity of the drug for its target, which could conceptually be achieved through short-range (primary resistance) or long-range (secondary resistance) effects. Mutation of residues in individual (or all) cluster zones could thus induce conformational modifications resulting in secondary resistance, or the compound could recognize multiple binding sites in L. Although not impossible, the nanomolar activity range of AS-136A renders at least the latter less likely. It is noteworthy in this context that NNRTI resistance mutations, as a rule of antiretroviral therapy, are typically located at the residues aligning the primary drug-binding pocket (14, 15). Little is known about the spatial organization of paramyxovirus L proteins. In analogy to structurally mapped NNRTI resistance mutations, it is intriguing to speculate that MeV L residues located in the three different resistance clusters (residues 589, 768/776, and 1239) may be part of a continuous microdomain in native L. This domain would include the GDNQ motif (residues 772 to 775) and thus bring the postulated RNA binding domain II (27) harboring residue 589, the conserved domain IV harboring residue 1239, and the proposed catalytic center for phosphodiester bond formation (10, 30) in proximity.

All mutations in L associated with resistance were found in conserved domains that show no genetic variance between a panel of currently endemic and attenuated MeV strains. This is consistent with our previous observation that no preexisting resistance against this drug class exists in a representative set of different wild-type MeV strains (57). Selective pressure to maintain the nature of these residues among MVi suggests a contribution of these residues to overall virus fitness, while most resistance mutations caused a delay in the onset of viral growth in cell culture to different degrees. In particular, in the case of a pathogen inducing predominantly acute disease, such as MeV, resistant variants harboring these mutations may be less pathogenic if they coincide with reduced efficiency of viral spread. Similarly, increased RdRp activity levels were previously linked to MeV attenuation (1). Resistance due to elevated polymerase activity may thus likewise reduce, rather than boost, viral pathogenicity and not impair the effectiveness of the AS-136A drug class.

This study confirms small-molecule targeting of RdRp components as an effective antiparamyxovirus strategy. Molecular characterization of viral escape mutants highlights the interaction of the AS-136A MeV inhibitor class with the viral L protein as the basis for inhibition. Two pathways of paramyxovirus escape from RdRp inhibition emerge: increased RdRp activity rates and, more frequently observed under our adaptation conditions, reduced drug sensitivity. Considering the balance between efficient viral replication and escape from the cellular antiviral response, either mechanism may compromise viral spread. Accordingly, small-molecule RdRp inhibitors targeting conserved domains of the complex appear particularly suitable for novel antiparamyxovirus therapies, since members of these families are associated predominantly with acute disease.

ACKNOWLEDGMENTS

We thank A. L. Hammond for critical reading of the manuscript.

This work was supported by U.S. Public Health Service grant AI071002 (to R.K.P.) from the NIH/NIAID.

REFERENCES

1. **Bankamp, B., S. P. Kearney, X. Liu, W. J. Bellini, and P. A. Rota.** 2002. Activity of polymerase proteins of vaccine and wild-type measles virus strains in a minigenome replication assay. J. Virol. **76:**7073–7081.
2. **Bose, S., and A. K. Banerjee.** 2004. Beta-catenin associates with human parainfluenza virus type 3 ribonucleoprotein complex and activates transcription of viral genome RNA in vitro. Gene Expr. **11:**241–249.
3. **Bowman, M. C., S. Smallwood, and S. A. Moyer.** 1999. Dissection of individual functions of the Sendai virus phosphoprotein in transcription. J. Virol. **73:**6474–6483.
4. **Buchholz, U. J., S. Finke, and K. K. Conzelmann.** 1999. Generation of bovine respiratory syncytial virus (BRSV) from cDNA: BRSV NS2 is not essential for virus replication in tissue culture, and the human RSV leader region acts as a functional BRSV genome promoter. J. Virol. **73:**251–259.
5. **Cattaneo, R., G. Rebmann, K. Baczko, V. ter Meulen, and M. A. Billeter.** 1987. Altered ratios of measles virus transcripts in diseased human brains. Virology **160:**523–526.
6. **Centers for Disease Control and Prevention.** 2008. Update: measles—United States, January-July 2008. MMWR Morb. Mortal. Wkly. Rep. **57:**893–896.
7. **Centers for Disease Control and Prevention.** 2008. Progress in global measles control and mortality reduction, 2000–2007. MMWR Morb. Mortal. Wkly. Rep. **57:**1303–1306.
8. **Cevik, B., D. E. Holmes, E. Vrotsos, J. A. Feller, S. Smallwood, and S. A. Moyer.** 2004. The phosphoprotein (P) and L binding sites reside in the N-terminus of the L subunit of the measles virus RNA polymerase. Virology **327:**297–306.
9. **Cevik, B., S. Smallwood, and S. A. Moyer.** 2007. Two N-terminal regions of the Sendai virus L RNA polymerase protein participate in oligomerization. Virology **363:**189–197.
10. **Chattopadhyay, A., T. Raha, and M. S. Shaila.** 2004. Effect of single amino acid mutations in the conserved GDNQ motif of L protein of rinderpest virus on RNA synthesis in vitro and in vivo. Virus Res. **99:**139–145.
11. **Chattopadhyay, A., and M. S. Shaila.** 2004. Rinderpest virus RNA polymerase subunits: mapping of mutual interacting domains on the large protein L and phosphoprotein p. Virus Genes **28:**169–178.
12. **Curran, J., T. Pelet, and D. Kolakofsky.** 1994. An acidic activation-like domain of the Sendai virus P protein is required for RNA synthesis and encapsidation. Virology **202:**875–884.
13. **De Clercq, E.** 2006. Antiviral agents active against influenza A viruses. Nat. Rev. Drug Discov. **5:**1015–1025.
14. **De Clercq, E.** 2004. Non-nucleoside reverse transcriptase inhibitors (NNRTIs): past, present, and future. Chem. Biodivers. **1:**44–64.
15. **De Clercq, E.** 1998. The role of non-nucleoside reverse transcriptase inhibitors (NNRTIs) in the therapy of HIV-1 infection. Antivir. Res. **38:**153–179.
16. **Doyle, J., A. Prussia, L. K. White, A. Sun, D. C. Liotta, J. P. Snyder, R. W. Compans, and R. K. Plemper.** 2006. Two domains that control prefusion stability and transport competence of the measles virus fusion protein. J. Virol. **80:**1524–1536.
17. **Dueweke, T. J., T. Pushkarskaya, S. M. Poppe, S. M. Swaney, J. Q. Zhao, I. S. Chen, M. Stevenson, and W. G. Tarpley.** 1993. A mutation in reverse

transcriptase of bis(heteroaryl)piperazine-resistant human immunodeficiency virus type 1 that confers increased sensitivity to other nonnucleoside inhibitors. Proc. Natl. Acad. Sci. USA **90:**4713–4717.
18. **European Centre for Disease Prevention and Control.** 3 July 2008, posting date. Measles once again endemic in the United Kingdom. http://www.eurosurveillance.org/ViewArticle.aspx?ArticleId=18919.
19. **Firsching, R., C. J. Buchholz, U. Schneider, R. Cattaneo, V. ter Meulen, and J. Schneider-Schaulies.** 1999. Measles virus spread by cell-cell contacts: uncoupling of contact-mediated receptor (CD46) downregulation from virus uptake. J. Virol. **73:**5265–5273.
20. **Griffin, D. E.** 2007. Measles virus, p. 1551–1585. *In* D. M. Knipe, P. M. Howley, D. E. Griffin, R. A. Lamb, M. A. Martin, B. Roizman, and S. E. Straus (ed.), Fields virology, 5th ed., vol. 1. Lippincott Williams & Wilkins, Philadelphia, PA.
21. **Hayden, F.** 2009. Developing new antiviral agents for influenza treatment: what does the future hold? Clin. Infect. Dis. **48**(Suppl. 1)**:**S3–S13.
22. **Hilleman, M. R.** 2001. Current overview of the pathogenesis and prophylaxis of measles with focus on practical implications. Vaccine **20:**651–665.
23. **Holmes, D. E., and S. A. Moyer.** 2002. The phosphoprotein (P) binding site resides in the N terminus of the L polymerase subunit of Sendai virus. J. Virol. **76:**3078–3083.
24. **Horikami, S. M., J. Curran, D. Kolakofsky, and S. A. Moyer.** 1992. Complexes of Sendai virus NP-P and P-L proteins are required for defective interfering particle genome replication in vitro. J. Virol. **66:**4901–4908.
25. **Katz, S. L.** 2006. Polio—new challenges in 2006. J. Clin. Virol. **36:**163–165.
26. **Kremer, J. R., and C. P. Muller.** 2009. Measles in Europe—there is room for improvement. Lancet **373:**356–358.
27. **Lamb, R. A., and G. D. Parks.** 2007. Paramyxoviridae: the viruses and their replication, p. 1449–1496. *In* D. M. Knipe, P. M. Howley, D. E. Griffin, R. A. Lamb, M. A. Martin, B. Roizman, and S. E. Straus (ed.), Fields virology, 5th ed., vol. 1. Lippincott Williams & Wilkins, Philadelphia, PA.
28. **Lee, J. K., A. Prussia, J. P. Snyder, and R. K. Plemper.** 2007. Reversible inhibition of the fusion activity of measles virus F protein by an engineered intersubunit disulfide bridge. J. Virol. **81:**8821–8826.
29. **Liu, X., B. Bankamp, W. Xu, W. J. Bellini, and P. A. Rota.** 2006. The genomic termini of wild-type and vaccine strains of measles virus. Virus Res. **122:**78–84.
30. **Malur, A. G., N. K. Gupta, P. De Bishnu, and A. K. Banerjee.** 2002. Analysis of the mutations in the active site of the RNA-dependent RNA polymerase of human parainfluenza virus type 3 (HPIV3). Gene Expr. **10:**93–100.
31. **Mellors, J. W., G. E. Dutschman, G. J. Im, E. Tramontano, S. R. Winkler, and Y. C. Cheng.** 1992. In vitro selection and molecular characterization of human immunodeficiency virus-1 resistant to non-nucleoside inhibitors of reverse transcriptase. Mol. Pharmacol. **41:**446–451.
32. **Moss, W. J., and D. E. Griffin.** 2006. Global measles elimination. Nat. Rev. Microbiol. **4:**900–908.
33. **Moyer, S. A., S. C. Baker, and S. M. Horikami.** 1990. Host cell proteins required for measles virus reproduction. J. Gen. Virol. **71:**775–783.
34. **Moyer, S. A., S. C. Baker, and J. L. Lessard.** 1986. Tubulin: a factor necessary for the synthesis of both Sendai virus and vesicular stomatitis virus RNAs. Proc. Natl. Acad. Sci. USA **83:**5405–5409.
35. **Oberg, B.** 2006. Rational design of polymerase inhibitors as antiviral drugs. Antivir. Res. **71:**90–95.
36. **Ono, N., H. Tatsuo, Y. Hidaka, T. Aoki, H. Minagawa, and Y. Yanagi.** 2001. Measles viruses on throat swabs from measles patients use signaling lymphocytic activation molecule (CDw150) but not CD46 as a cellular receptor. J. Virol. **75:**4399–4401.
37. **Orenstein, W. A., M. J. Papania, and M. E. Wharton.** 2004. Measles elimination in the United States. J. Infect. Dis. **189**(Suppl. 1)**:**S1–S3.
38. **Orenstein, W. A., P. M. Strebel, M. Papania, R. W. Sutter, W. J. Bellini, and S. L. Cochi.** 2000. Measles eradication: is it in our future? Am. J. Public Health **90:**1521–1525.
39. **Palese, P., and M. L. Shaw.** 2007. Orthomyxoviridae: the viruses and their replication, p. 1647–1690. *In* D. M. Knipe, P. M. Howley, D. E. Griffin, R. A. Lamb, M. A. Martin, B. Roizman, and S. E. Straus (ed.), Fields virology, 5th ed., vol. 2. Lippincott Williams & Wilkins, Philadelphia, PA.
40. **Parks, G. D.** 1994. Mapping of a region of the paramyxovirus L protein required for the formation of a stable complex with the viral phosphoprotein P. J. Virol. **68:**4862–4872.
41. **Plemper, R. K., J. Doyle, A. Sun, A. Prussia, L. T. Cheng, P. A. Rota, D. C. Liotta, J. P. Snyder, and R. W. Compans.** 2005. Design of a small-molecule entry inhibitor with activity against primary measles virus strains. Antimicrob. Agents Chemother. **49:**3755–3761.
42. **Plemper, R. K., K. J. Erlandson, A. S. Lakdawala, A. Sun, A. Prussia, J. Boonsombat, E. Aki-Sener, I. Yalcin, I. Yildiz, O. Temiz-Arpaci, B. Tekiner, D. C. Liotta, J. P. Snyder, and R. W. Compans.** 2004. A target site for template-based design of measles virus entry inhibitors. Proc. Natl. Acad. Sci. USA **101:**5628–5633.
43. **Plemper, R. K., A. L. Hammond, D. Gerlier, A. K. Fielding, and R. Cattaneo.** 2002. Strength of envelope protein interaction modulates cytopathicity of measles virus. J. Virol. **76:**5051–5061.
44. **Prussia, A. J., R. K. Plemper, and J. P. Snyder.** 2008. Measles virus entry inhibitors: a structural proposal for mechanism of action and the development of resistance. Biochemistry **47:**13573–13583.
45. **Radecke, F., P. Spielhofer, H. Schneider, K. Kaelin, M. Huber, C. Dotsch, G. Christiansen, and M. A. Billeter.** 1995. Rescue of measles viruses from cloned DNA. EMBO J. **14:**5773–5784.
46. **Richman, D., C. K. Shih, I. Lowy, J. Rose, P. Prodanovich, S. Goff, and J. Griffin.** 1991. Human immunodeficiency virus type 1 mutants resistant to nonnucleoside inhibitors of reverse transcriptase arise in tissue culture. Proc. Natl. Acad. Sci. USA **88:**11241–11245.
47. **Rota, P. A., D. A. Featherstone, and W. J. Bellini.** 2009. Molecular epidemiology of measles virus. Curr. Top. Microbiol. Immunol. **330:**129–150.
48. **Ryan, K. W., E. M. Morgan, and A. Portner.** 1991. Two noncontiguous regions of Sendai virus P protein combine to form a single nucleocapsid binding domain. Virology **180:**126–134.
49. **Sidhu, M. S., J. Chan, K. Kaelin, P. Spielhofer, F. Radecke, H. Schneider, M. Masurekar, P. C. Dowling, M. A. Billeter, and S. A. Udem.** 1995. Rescue of synthetic measles virus minireplicons: measles genomic termini direct efficient expression and propagation of a reporter gene. Virology **208:**800–807.
50. **Spearman, C.** 1908. The method of right and wrong cases (constant stimuli) without Gauss's formula. Br. J. Psychol. **2:**227–242.
51. **Statens Serum Institut.** 16 July 2008, posting date. Measles surveillance first quarterly report 2008. http://www.euvac.net/graphics/euvac/pdf/2008_first.pdf.
52. **Statens Serum Institut.** 10 September 2008, posting date. Measles surveillance second quarterly report 2008. http://www.euvac.net/graphics/euvac/pdf/2008_second.pdf.
53. **Sun, A., N. Chandrakumar, J. J. Yoon, R. K. Plemper, and J. P. Snyder.** 2007. Non-nucleoside inhibitors of the measles virus RNA-dependent RNA polymerase complex activity: synthesis and in vitro evaluation. Bioorg. Med. Chem. Lett. **17:**5199–5203.
54. **Sun, A., J. J. Yoon, Y. Yin, A. Prussia, Y. Yang, J. Min, R. K. Plemper, and J. P. Snyder.** 2008. Potent non-nucleoside inhibitors of the measles virus RNA-dependent RNA polymerase complex. J. Med. Chem. **51:**3731–3741.
55. **Tan, S. L., G. Ganji, B. Paeper, S. Proll, and M. G. Katze.** 2007. Systems biology and the host response to viral infection. Nat. Biotechnol. **25:**1383–1389.
56. **United Kingdom Health Protection Agency.** 28 November 2008, posting date. Health protection report. Confirmed measles cases in England and Wales—an update to the end of October 2008. http://www.hpa.org.uk/hpr/archives/2008/news4808.htm#measles.
57. **White, L. K., J. J. Yoon, J. K. Lee, A. Sun, Y. Du, H. Fu, J. P. Snyder, and R. K. Plemper.** 2007. Nonnucleoside inhibitor of measles virus RNA-dependent RNA polymerase complex activity. Antimicrob. Agents Chemother. **51:**2293–2303.
58. **World Health Organization.** 1998. Expanded programme on immunization (EPI). Wkly. Epidemiol. Rec. **73:**265–272.